Biophysical Journal Volume 108 March 2015 1220–1228

Article

Crowding Induces Complex Ergodic Diffusion and Dynamic Elongation of Large DNA Molecules

Cole D. Chapman,[2] Stephanie Gorczyca,[1] and Rae M. Robertson-Anderson[1,*]

[1]Department of Physics, University of San Diego, San Diego, California; and [2]Department of Physics, University of California San Diego, La Jolla, California

ABSTRACT Despite the ubiquity of molecular crowding in living cells, the effects of crowding on the dynamics of genome-sized DNA are poorly understood. Here, we track single, fluorescent-labeled large DNA molecules (11, 115 kbp) diffusing in dextran solutions that mimic intracellular crowding conditions (0–40%), and determine the effects of crowding on both DNA mobility and conformation. Both DNAs exhibit ergodic Brownian motion and comparable mobility reduction in all conditions; however, crowder size (10 vs. 500 kDa) plays a critical role in the underlying diffusive mechanisms and dependence on crowder concentration. Surprisingly, in 10-kDa dextran, crowder influence saturates at ~20% with an ~5× drop in DNA diffusion, in stark contrast to exponentially retarded mobility, coupled to weak anomalous subdiffusion, with increasing concentration of 500-kDa dextran. Both DNAs elongate into lower-entropy states (compared to random coil conformations) when crowded, with elongation states that are gamma distributed and fluctuate in time. However, the broadness of the distribution of states and the time-dependence and length scale of elongation length fluctuations depend on both DNA and crowder size with concentration having surprisingly little impact. Results collectively show that mobility reduction and coil elongation of large crowded DNAs are due to a complex interplay between entropic effects and crowder mobility. Although elongation and initial mobility retardation are driven by depletion interactions, subdiffusive dynamics, and the drastic exponential slowing of DNA, up to ~300×, arise from the reduced mobility of larger crowders. Our results elucidate the highly important and widely debated effects of cellular crowding on genome-sized DNA.

INTRODUCTION

Biological cells, comprised of a wide range of macromolecules of varying sizes and structures, are highly crowded, with typical concentrations of ~200–400 mg/mL (20–40% w/v) (1). Crowding has been shown to play a principle role in a wide array of biological processes, such as gene expression, protein folding, binding and aggregation, chromosomal compaction, cell volume regulation, and catalytic enzyme activity (1–6). Drug delivery systems, gene therapy, and production and manipulation of synthetic cells and nanomaterials are also highly impacted by cellular crowding (2,3,7,8). Macromolecular mobility is greatly reduced in crowded environments, yet despite these extreme conditions, diffusion is the primary mechanism by which the majority of reactions and interactions occur. Further, crowding has been shown to alter the conformations and stability of nucleic acids and proteins, which greatly impact protein-DNA binding efficiency, transcription, and replication (3,8). Despite the obvious importance of understanding molecular diffusion and configuration in crowded environments, the sheer system complexity, coupled with conflicting experimental and theoretical studies (3,9), leaves this open problem widely debated by a range of researchers in biology, physics, engineering, materials science, and medicine.

Genomic DNA, storing the genetic code for almost all living things and playing a pivotal role in several other biological functions (10,11), varies widely in size and conformation among living organisms and is often one of the largest macromolecules in the cell (with bacterial genomes ranging from ~10–10,000 kbp). While DNA is often bound by histones or other DNA-binding proteins, there are a number of very important biological processes and biomedical and biotechnology advances that depend on the transport of naked DNA. Several important examples that have received much recent attention include nonviral gene delivery and antisense therapy, transfection and transformation, and DNA replication and transcription (12–14). Despite the complexity and significance of large naked DNA, there is a paucity of studies investigating how cellular crowding levels impact the mobility and configuration of large DNA molecules.

Here, we use single-molecule fluorescence microscopy and particle-tracking techniques to simultaneously characterize the diffusion and conformations of large double-stranded DNA molecules (11 and 115 kbp) in 0–40% solutions of dextran (10 and 500 kDa), a widely used inert crowder comparable in size to small proteins (15). For each case, we quantify mean squared displacements and

Submitted October 3, 2014, and accepted for publication February 2, 2015.

*Correspondence: randerson@sandiego.edu

Editor: Keir Neuman.

0006-3495/15/03/1220/9 $2.00

http://dx.doi.org/10.1016/j.bpj.2015.02.002

corresponding diffusion coefficients and ergodicity of DNA motion. We simultaneously determine the degree of conformational state change of DNA upon crowding, as well as corresponding probability distributions and time-dependent fluctuations of states.

Varying experimental and simulation results have been reported regarding the diffusion of macromolecules within crowded environments. Diffusion measurements of small DNA fragments (<4.5 kbp) in up to 40% Ficoll-70 (16) and the cytoplasm and nucleus of HeLa cells (17), large (48 kbp) DNA in dilute dextran solutions confined within a nanochannel (18), and apomyoglobin in RNase and human serum albumin (19) have all reported normal Brownian motion where the mean-squared displacement (MSD) can be used to calculate the diffusion coefficient via MSD $= 2Dt$. In contrast, several groups have found evidence of anomalous diffusion in crowded systems, where MSD ~ t^{α} with typical α-values of 0.7–0.9 (i.e., subdiffusion) (9). Such anomalous behavior has been reported for aptoferrin in 500-kDa dextran (20), microspheres in cytoplasm (21), nanoparticles in dextran (22), and micron-sized Cajal bodies in the nucleus of HeLa cells (23). Small single-stranded DNA in 10-kDa dextran solutions at cellular concentrations was also found to be subdiffusive ($\alpha \geq 0.7$) (24).

While crowding is known to greatly impact the conformations of macromolecules, few studies have examined the effects of crowding on DNA conformation and have reported varying results. In crowded blends of DNA and polyethylene glycol, DNA has been shown to undergo compaction at low DNA concentrations and elongation and phase separation at high DNA concentrations (25,26). Conversely, DNA molecules confined within nanogeometries and crowded by dextran have been shown to swell, elongate, or compact depending on the confinement geometry, crowding level, and ionic conditions (6,18,27). The time-dependence and length scale of conformational state fluctuations within crowded environments remains unknown.

Thus, in comparison to their ubiquity and heavy biological significance, the effects of crowding on DNA are poorly understood. As such, our described experiments address important unanswered questions by elucidating the molecular level effects of cellular crowding on both the dynamics and configurational states of genome-sized DNA and the connection between center-of-mass mobility and conformational dynamics.

MATERIALS AND METHODS

Double-stranded 11- and 115-kbp DNA were prepared, as previously described in Laib et al. (28), by replication of cloned plasmid (11 kbp) and bacterial artificial chromosome (115 kbp) constructs in *Escherichia coli*, followed by extraction, purification, and restriction enzyme treatment to convert supercoiled constructs to linear form. For measurements, solutions of 10- and 500-kDa dextran (Sigma-Aldrich, St. Louis, MO) at concentrations of 0, 10, 20, 30, and 40% w/v were prepared in aqueous buffer (10 mM Tris-HCl (pH 8), 1 mM EDTA, 10 mM NaCl). Trace amounts of either 11- or 115-kbp DNA, uniformly labeled with YOYO-1 (Invitrogen, Carlsbad, CA), were mixed into dextran solutions, loaded into sample chambers, and equilibrated for ~30 min before measurements.

Using a high-speed charge-coupled device QImaging camera on an Eclipse A1R inverted microscope (Nikon, Melville, NY), videos ranging from 5 to 60 s of DNA diffusing within dextran solutions were recorded at 10 frames/s. Approximately 150–300 DNA molecules were recorded for each case. Custom-written software (done in MATLAB; The MathWorks, Natick, MA) was implemented to track the 1) center of mass position and 2) major axis (R_{max}) and minor axis (R_{min}) vectors for each molecule (as described in Results and Discussion). Tracked trajectories were then used to calculate all presented quantities (Figs. 1, 2, 3, 4, and 5). Error for MSDs and D values were calculated using the bootstrap method (29).

The zero-shear viscosity of dextran solutions of different concentrations were measured using optical tweezers microrheology as described previously in Chapman et al. (30). Briefly, microspheres of radius $r = 2.25$ μm embedded in dextran solutions were trapped and oscillated over a range of small amplitude frequencies (0.5 μm; 0.05–10.0 Hz) using an optical tweezers and piezoelectric microscope stage. Microspheres were coated with BSA to prevent nonspecific binding. Oscillation amplitudes and frequencies were low enough to ensure we were probing the near-equilibrium properties of the solution such that inhomogeneities in the flow field and depletion around the bead are negligible (30,31). The force F that the dextran solution exerts on the oscillating sphere was measured using a position-sensing detector that measures the deflection of the trapping laser during oscillation. The measured force on the sphere and speed v of the piezoelectric stage were used to determine the viscosity via Stokes drag ($F = 6\pi\eta rv$ where η is the solution viscosity). Further measurement details are fully described and justified in Chapman et al. (30) and Chapman and Robertson-Anderson (31). Some of the higher concentration viscosities exhibit modest frequency dependence (shear thinning) at higher frequencies, but all solutions reach a low frequency plateau (see Fig. S1 in the Supporting Material). We determine the zero-shear viscosity from this low frequency plateau value of viscosity. Measured viscosities are presented in Fig. S1.

RESULTS AND DISCUSSION

Diffusion

We have imaged single, fluorescent-labeled DNA molecules diffusing in dextran solutions of concentrations, C, comparable to cellular conditions ($C = 0$–40 (% w/v)). We tracked the center-of-mass positions of ~150–300 diffusing DNA in time to quantify the MSDs for each case (Fig. 1). For each MSD, we evaluate α, where MSD ~ t^{α}, and, as expected, for DNA diffusing in the absence of crowders ($C = 0$), we find purely linear behavior (i.e., classical Brownian motion) for all measured timescales (0.1–10 s and 10–50 s). We also find α ~ 1 for DNA diffusing in 10-kDa dextran (S_d) for all DNA lengths, crowding concentrations, and timescales. Conversely, 0.1–10 s MSDs for both DNA constructs in 500-kDa dextran (L_d) solutions exhibit weakly anomalous mobility with α-values of ~0.66 $\pm$ 0.05–0.87 $\pm$ 0.06, decreasing slightly with increasing C (Fig. 1 *A*). Our results suggest that the crowder size, rather than DNA size, plays the key role in the emergence of subdiffusive dynamics.

Multiple models have been proposed to explain the source of anomalous subdiffusion within crowded environments, with the two most widely invoked being the

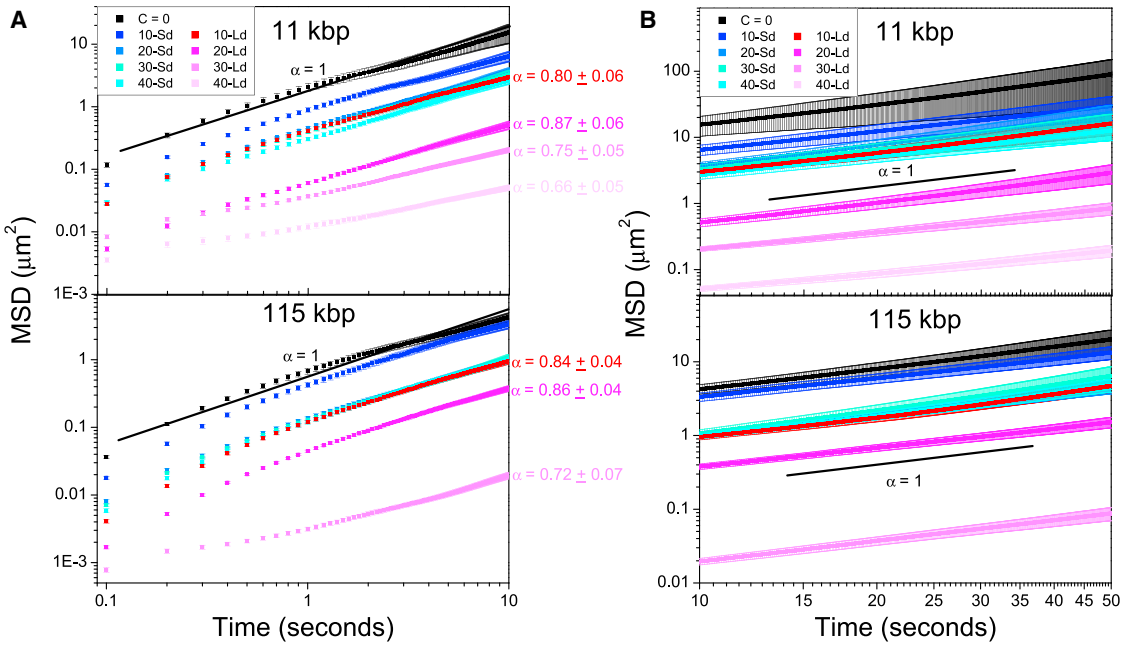

FIGURE 1 Mean-squared displacements versus time for the 11-kbp (*top*) and 115-kbp (*bottom*) DNA diffusing in both 10-kDa (S_d) and 500-kDa (L_d) dextran from (*A*) 0.1–10 s and (*B*) 10–50 s. The concentration, *C* (% w/v), and crowder size (S_d or L_d) for each MSD is indicated in the legend. (*A*) All MSDs are fit to a power law MSD ~ t^{α}. $\alpha = 1$ scaling (*black line*), which demonstrates classical Brownian motion, is added for convenience. For cases that display sublinear scaling, α-values are listed to the right of the MSD in the corresponding color. MSDs without a listed α-value display linear scaling. (*B*) For long timescales, α approaches unity for all cases. To see this figure in color, go online.

continuous time random walk and fractional Brownian motion (FBM) models (20,32–34). The continuous time random walk is built around a non-Gaussian propagator, and reveals distinctly nonergodic behavior, where time-averaged MSDs differ from ensemble-averaged MSDs (32). FBM, on the other hand, is completely ergodic with diffusion driven by a stationary Gaussian process (9,32). Thus, to determine which model describes our weakly anomalous behavior, we test the ergodicity of the DNA diffusion by evaluating the two most robust ergodicity-breaking parameters (34),

$$EB(t) = \frac{\overline{\langle \delta^2(t) \rangle}}{\langle x^2(t) \rangle}$$

and the non-Gaussianity parameter,

$$G(t) = \frac{1}{2} \frac{\overline{\langle \delta^4(t) \rangle}}{\left\langle \overline{\delta^2(t)} \right\rangle^2} - 1,$$

where $\langle x^2(t) \rangle$ is the MSD and $\overline{\langle \delta^2(t) \rangle}$ is the time-averaged MSD. For a purely Gaussian ergodic process, $EB = 1$ and $G \rightarrow 0$ for sufficiently long times. For all data sets measured, we find that G goes to zero and $EB \sim 1$ (Fig. 2) (34). Thus our results show that large DNA diffusion is best modeled by FBM, which is a Gaussian stationary process. We note that obstructed diffusion is another potential ergodic process that has been proposed for crowded environments (9), but this model is based on immobile crowders. Thus, obstructed diffusion should only explain cases in which the diffusion timescale of the crowders is much slower than that of the diffusing molecule, whereas in our experiments the crowders are much more mobile than the DNA itself. The radii of gyration of S_d and L_d are

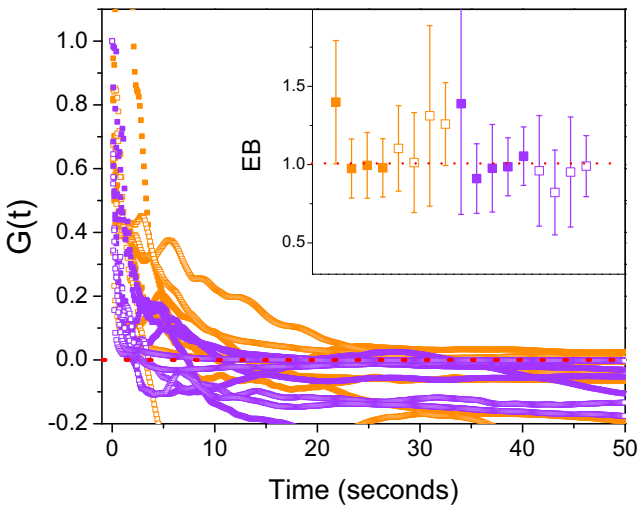

FIGURE 2 Non-Gaussianity parameter, *G* versus time for 11-kbp (*purple*) and 115-kbp (*orange*) DNA diffusing in 10-kDa (*open squares*) and 500-kDa (*solid squares*) dextran. Note that G tends to zero (*dashed line*), indicating an ergodic diffusion process. (*Inset*) Calculated ergodicity-breaking term (*EB*) for each crowding case. $EB = 1$ (*dashed line*) indicates ergodic behavior. See text for definitions of *G* and *EB*. To see this figure in color, go online.

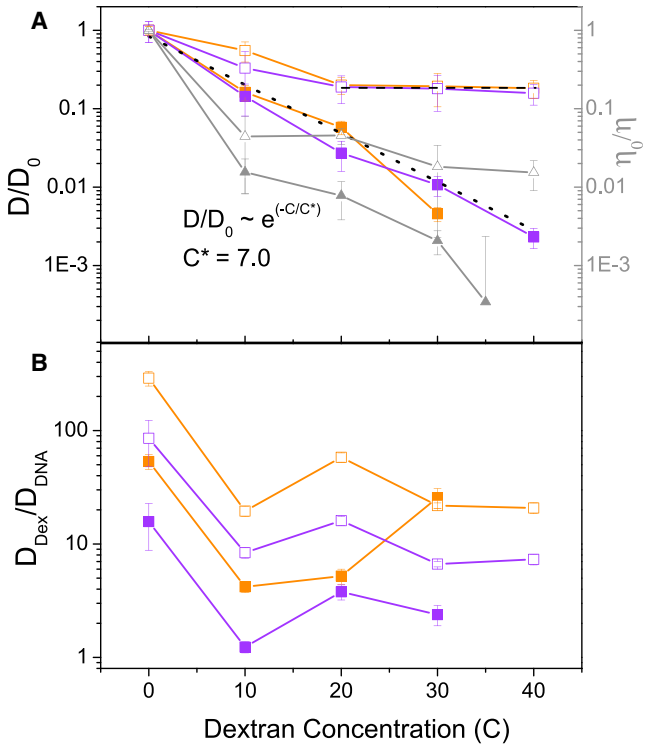

FIGURE 3 (*A*) Normalized DNA diffusion coefficients, D/D_0, and inverse normalized dextran solution viscosities, η_0/η, versus dextran concentration C (% w/v) for DNA diffusing in dextran solutions. Color and symbol scheme is as in Fig. 2 (inverse viscosity shown in *gray*). The reduction in D from $C = 0$ (D_0) appears independent of DNA length with the crowder length playing a dominating role. Note the surprising saturating effect for 10-kDa dextran data with negligible change in D/D_0 for $C > 20$ (*horizontal dashed line*). Conversely, in 500 kDa, D/D_0 displays exponential scaling with C. From the exponential fit (*dotted line*), we find a critical crowding concentration of C^* ~7.0. (*B*) Ratio of dextran versus DNA diffusion coefficients for each crowding case (same color/symbol scheme as in *A*). To see this figure in color, go online.

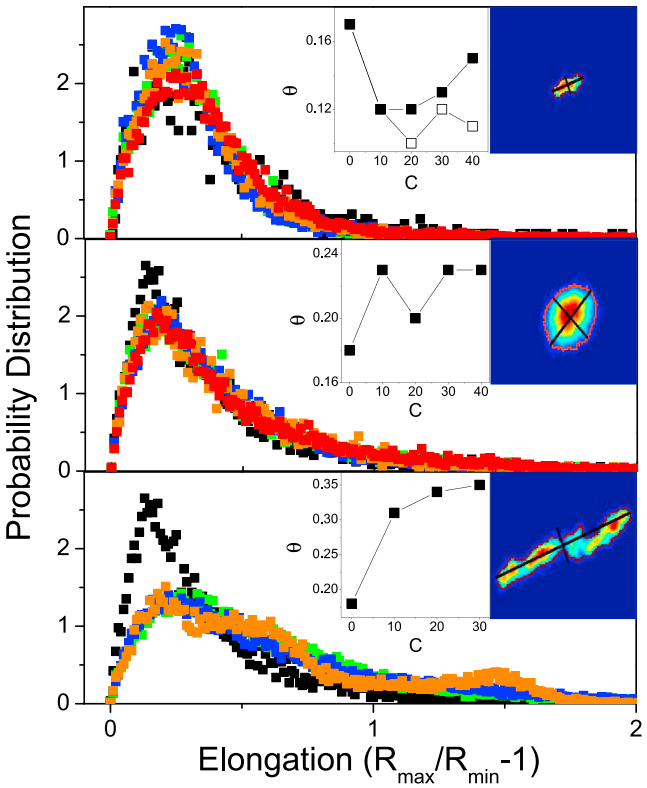

FIGURE 4 Probability distributions for elongation parameter E for 11-kbp DNA in 500-kDa dextran (*top*), 115-kbp DNA in 10-kDa dextran (*middle*), and 115-kbp DNA in 500-kDa dextran (*bottom*). Distributions for $C = 0$ (*black*), 10 (*green*), 20 (*blue*), 30 (*orange*), and 40 (*red*) are shown. *Right insets* show recorded images ($(10\ \mu m)^2$) of typical DNA conformations when crowded. DNA outline and major (R_{max}) and minor (R_{min}) axes used to calculate E are shown. (*Left insets*) Gamma-distribution width parameter (θ) versus C. For 115-kbp DNA, this width is lowest for $C = 0$ while for 11-kbp DNA, θ at $C = 0$ is highest. The distribution for 11-kbp DNA in 10-kDa dextran (not shown) is nearly identical to that in 500-kDa dextran (*top*). The θ values for this case are shown (*open squares*, *top inset*). To see this figure in color, go online.

$R_g = 3.5$ and 19 nm, respectively (18), as compared to our DNA, which have $R_g = 0.2$ and 1.0 μm for the 11- and 115-kbp DNA (35). Using our measured viscosities of the different dextran solutions, we can calculate the diffusion coefficients for dextran via $D = k_bT/6\pi\eta R_g$ and compare to those of our DNA (see Fig. 3 *B*). As seen in Fig. 3 *B*, even L_d diffuses ~5× times faster than the 11-kbp DNA, and in most cases dextran is diffusing ~10–100× times faster. Thus, dextran behaves as a relatively mobile crowder compared to the timescale of DNA mobility.

Finally, another possible explanation for our measured subdiffusion is that the DNA is trapped in minima surrounded by the crowders, which would have to collectively move before DNA can diffuse (36,37). However, the studies that have reported this source of subdiffusion also find that the trapped polymer undergoes compaction. In our conformational analysis (described in Conformation, below), we see no signs of compaction; instead, we observe polymer elongation, so we believe that this explanation is likely not valid for our experimental parameters.

Crowding-induced subdiffusion is predicted to only be apparent at intermediate timescales and approach normal diffusion on long timescales (9). Using this prediction, coupled with the weak nature and ergodicity of the subdiffusion, we approximate our MSDs in L_d at long times (10–50 s; Fig. 1 *B*) as linear to extract diffusion coefficients D and compare to D values found in S_d (Fig. 3). Importantly, α-values determined from these long-time tails of the MSDs are all indistinguishable from unity within the experimental error, demonstrating the accuracy of the reported D values (Fig. 1 *B*).

We find that the reduction of D from the $C = 0$ case (D_0), as concentration of either crowder increases, is nearly identical for both DNA lengths; however, the concentration dependence of D/D_0 is starkly different in S_d versus L_d, once again demonstrating that DNA mobility is driven by crowder size rather than DNA size. We note that a reduction in mobility with increasing concentration is not entirely

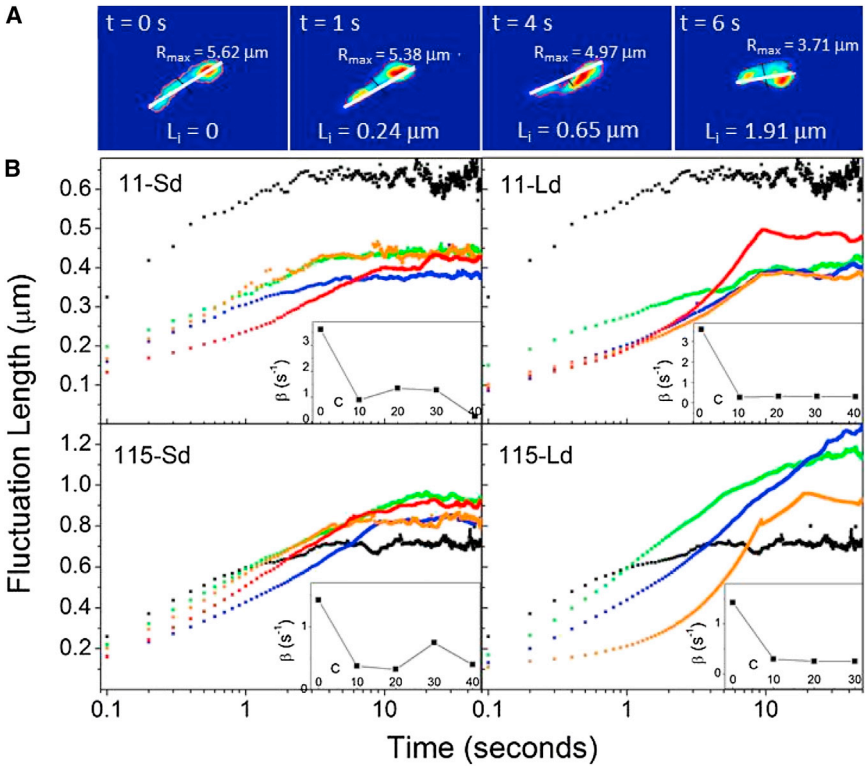

FIGURE 5 (*A*) Measured major axis, R_{max} (*white line*) and minor axis, R_{min} (*black line*) for a typical 115-kbp DNA molecule diffusing in L_d ($C = 20$) with increasing time. The fluctuation length for the displayed molecule, L_i, is noted for each frame. (*B*) Ensemble-averaged fluctuation length, L, versus time for 11-kbp DNA in 10-kDa dextran (11 S_d), 11-kbp DNA in 500-kDa dextran (11 L_d), 115-kbp DNA in 10-kDa dextran (115 S_d), and 115-kbp DNA in 500-kDa dextran (115 L_d). Color scheme is the same as in Fig. 4. (*Insets*) Fluctuation lengths are all fit to single exponentials with decay rate value β. The decay rate for $C = 0$ is highest for all cases, as expected; however, it remains relatively unchanged as C increases beyond 10. Also note that the terminal fluctuation length, ~0.7 μm for both DNAs at $C = 0$, increases ~46% for 115-kbp DNA upon crowding but actually decreases ~40% for 11-kbp DNA. To see this figure in color, go online.

surprising, and could in fact simply be due to the increasing viscosity of the L_d and S_d solutions with increasing concentration via the Stokes-Einstein relation $D \sim \eta^{-1}$. To separate the effect of increasing viscosity with dextran concentration from our measured mobility reduction, we compare D/D_0 to η_0/η (Fig. 3 *A*). As seen is Fig. 3 *A*, we find that crowding-induced mobility reduction is distinctly different from that due simply to increasing viscosity.

We find that the DNA mobility is actually enhanced compared to that expected from Stokes-Einstein dynamics. This enhanced mobility takes effect immediately at the onset of crowding ($C = 10$) with the DNA exhibiting a mobility ~10× faster than its corresponding Stokes-Einstein mobility. This effect can also be seen by comparing dextran diffusion coefficients D_{dex} to that of DNA (Fig. 3 *B*). If the DNA mobility reduction were purely viscosity-dependent, then D_{dex}/D_{DNA} would remain constant for all concentrations. However, as seen in Fig. 3 *B*, this ratio initially drops an order of magnitude (enhanced DNA mobility) then remains relatively constant, with a modest increase for L_d solutions and decrease for S_d solutions as C increases. We can understand this enhanced mobility as arising from the corresponding conformational change of the DNA that we observe at the onset of crowding (see Conformation below). The DNA undergoes a conformational change to facilitate transport through the crowded solution. Note that both the relative mobility enhancement and the conformational change appear at the onset of crowding and remain relatively unchanged as the crowding increases.

We find that in S_d, DNA mobility is reduced ~5× from $C = 0$–20 compared to the ~20× increase in viscosity; however, surprisingly, for $C > 20$, a saturating effect is observed as D/D_0 remains nearly constant for both lengths of DNA while the viscosity increases ~3× more. To our knowledge, this is the first time such a saturating effect has been reported for diffusion in a crowded system. We note that this result appears counterintuitive according to the Stokes-Einstein fluid relation $D \sim \eta^{-1}$, and given the error in our measured D values, it is possible that the mobility is actually decreasing with increasing C, albeit with a weak dependence that is immeasurable within our experimental error. As described above, we interpret this result as arising from the change in conformational dynamics of the DNA that we observe upon crowding as detailed in the following Conformation section. The change in DNA conformation and the associated fluctuations directly impact the COM diffusion, and could lead to enhanced mobility as compared to that due to fluid viscosity, as described above.

Conversely, in L_d, we find D/D_0 for both DNA constructs decreases exponentially up to the highest C values, dropping by ~300, though still significantly enhanced in comparison to the ~3000× increase in viscosity. By fitting the data to an exponential of the form $D/D_0 \sim \exp(-C/C^*)$, we find a critical crowding concentration of $C^* = 7.0\%$. Because the mobility reduction deviates from the viscosity relation at ~C^*, we can interpret our measured critical crowding concentration as quantifying the concentration at which crowding induces breakdown of Stokes-Einstein mobility

of DNA. Further, the concentration at which we begin to observe weak subdiffusion in L_d is ~$2C^*$, once again demonstrating that the dependence of diffusion on crowding concentration cannot be explained by Stokes-Einstein fluid effects. Similar results, namely DNA-independent mobility reduction and exponential dependence on C, have been reported for shorter DNA (<4.5 kbp) in Ficoll-70 (16).

The significant difference in diffusive dynamics of DNA between S_d and L_d cases can be understood by noting the significant difference in mobility of the two crowders (Fig. 3). While highly mobile crowders (i.e., S_d is ~60× and ~300× more mobile than 11 and 115 kbp DNA) contribute to reduced mobility, this effect alone cannot explain the extreme mobility reduction seen with L_d and in many other crowded systems (16,21,24).

Interestingly, our results are distinctly different from our previous diffusion results for semidilute and concentrated solutions of large DNA (38,39), which show power law dependence on solution concentration as well as a strong dependence on DNA length in line with classical Doi-Edwards polymer theory (40). Further, we previously found no evidence of subdiffusion despite the fact that actual D values were comparable in magnitude to those measured in this study. This sharp contrast indicates that crowded systems, comprised of molecules with different sizes and structures, have unique and complex dynamics not explained by classical theory for concentrated homogenous polymer solutions.

Conformation

To further elucidate the effects of crowding on DNA, we investigated the conformational changes induced by S_d and L_d. During measurements, we commonly observed an unexpected elongation of DNA relative to the dilute case ($C = 0$), where DNA assumes a roughly spherical random coil conformation (Fig. 4, *insets*; Fig. 5 *A*). To quantify this elongation, which was most apparent for 115-kbp DNA in L_d, we use custom-written software (MATLAB) to quantify a major (R_{max}) and minor (R_{min}) axis (Fig. 4, *insets*) of each DNA molecule for all recorded frames. The method we use that defines an outline of the molecule is similar to that of calculating the radius of gyration tensor for each conformation (41). From our measured major and minor axes, we define an elongation parameter, $E = (R_{max}/R_{min}) - 1$, to quantify the elongation relative to the random coil state. We find that the probability distribution of elongation states P_E is well fit to a gamma-distribution,

$$P_E(k,\theta) = \frac{\theta^{-k}}{\Gamma(k)} E^{k-1} e^{\frac{-E}{\theta}},$$

where k is the shape term and θ is a measure of the distribution width (Fig. 4). Gamma-distributions have also recently been shown to describe the dynamics of several biological processes dominated by Brownian motion (42,43).

For 115-kbp DNA in L_d, we see an ~67% increase in the average elongation coupled with a distribution widening of $\theta \approx 0.37$ for $C = 0$ to $\theta \approx 0.62$ for all crowding levels. Similar behavior (C-independent elongation and distribution widening) is seen for 115-kbp DNA in S_d, although it is less pronounced. Interestingly, while we find modest elongation for the 11-kbp DNA (similar to 115-kbp DNA in S_d), the distribution width θ actually decreases with the addition of dextran (Fig. 4, *inset*). Of note is the saturation effect of elongation for both DNAs, as the initial addition of dextran ($C = 10$) causes an increase in the average elongation and change in distribution width but this distribution remains relatively unchanged up to the highest concentration (Fig. 4). Elongation has only previously been reported for crowded DNA when confined in nanogeometries (18,27) or in conjunction with large-scale phase separation (26) at high salt conditions.

We also sought to determine whether the elongation distributions arise from an ensemble of individual molecules, each with relatively fixed elongation states that varied from molecule to molecule, or from individual molecules (all in similar states) fluctuating between elongation states in time. Thus, to evaluate the time dependence of elongation, we define a fluctuation length,

$$L(t) = \langle |R_{max}(0) - R_{max}(t)| \rangle,$$

which quantifies how quickly the conformational state of a molecule is changing and the length scale of elongation fluctuations. Fig. 5 *A* depicts the physical interpretation of $L(t)$, and demonstrates that for very short times $L(t)$ is nearly zero because the DNA has not had time to alter its conformation. As t increases, the conformation changes more apparently. For long times, $L(t)$ approximately plateaus to a near steady-state terminal value, L_p (Fig. 5 *B*). We can understand this terminal value as the length scale of conformational breathing between different states. By fitting $L(t)$ to a single exponential we quantify a decay rate, β, for conformational breathing, or the rate at which elongation states become decorrelated from one another (Fig. 5, *insets*). As expected, the decay rate of fluctuations is largest for $C = 0$ for all cases, indicating more rapid conformational fluctuations, which is then slowed, as DNA center-of-mass mobility is reduced by the addition of crowders.

Interestingly, we see once again a saturating effect with β decreasing upon initial crowding but remaining relatively unchanged for $C = 10$–40 for all DNA and crowder sizes, corroborating our elongation state distribution results. We are aware of no previously reported direct measure of the dynamics associated with crowding-induced conformational change. We note that a more conventional measure of correlations would be the autocorrelation function of the major axis in time, i.e., $\langle R(0)R(t) \rangle$. While this autocorrelation can provide the timescale of decorrelation,

similar to our measured decay rate, it does not provide a straightforward measure of the breathing length scale. Nonetheless, we calculate the autocorrelation of elongation states and find a similar decay rate (see Fig. S2), further validating our defined elongation fluctuation length parameter.

For the 115-kbp DNA, both in S_d and L_d, we find that the terminal fluctuation length, L_p, (~0.7 μm for $C = 0$) increases ~43% to ~1.0 μm for $C > 0$, indicating that the crowders are inducing larger, slower fluctuations. This result is in agreement with our elongation distribution data for 115-kbp DNA, where we indeed see an increased width in the gamma-distribution for $C > 0$ relative to $C = 0$. Interestingly, for 11 kbp in both S_d and L_d, L_p actually decreases ~40% upon crowding (from $L_p \approx 0.7$ μm at $C = 0$ to ~0.40 μm for $C > 0$), corroborated by the reduced width in elongation distribution upon crowding (Fig. 4). Thus our findings demonstrate, to our knowledge, a novel crowding-induced molecular elongation mechanism dominated by DNA size with crowder size also playing a role.

Naively, crowding-induced DNA elongation is counterintuitive, because the highest entropy state for DNA in solution is a random coil conformation. However, crowding-induced ordering of macromolecules is a well-known entropic effect of the depletion interaction as driven by entropy maximization of the crowders, which are much greater in number than the diffusing macromolecules of interest. The depletion interaction, whereby the crowders seek to increase their accessible volume and thus entropy, is responsible for a wide range of biochemical processes including enhanced protein folding and increased enzymatic reaction rates and DNA melting temperatures. When in a random coil, the spherical space taken up by the DNA is excluded from the dextran, which creates an effective osmotic pressure inward on the coil. While such pressure could lead to compaction at sufficiently high salt concentrations, the electrostatic repulsion of neighboring DNA segments prevents full compaction without high salt, so the DNA instead elongates to reduce the excluded volume. For reference, the volume taken up by a 115-kbp random coil with $R_g = 1$ μm is ~1 μm^3 compared to a volume of ~1 $\times$ 10^{-4} μm^3 (~(2 nm)^2 $\times$ 30 μm) for fully extended 115-kbp DNA. We see less pronounced elongation for S_d as these crowders are small enough that they could partially penetrate the random coil configuration, thereby lowering the osmotic pressure difference. While we see reduced elongation for 11-kbp DNA, we find that the width of the distribution of states is lowered along with the terminal fluctuation length. Both effects, signatures of increased order, reflect an alternative entropy minimizing induced in 11-kbp DNA by the crowders. Conversely, for 115-kbp DNA, because the elongation and corresponding entropy drop is much more extreme, it compensates partially by an increased width of distribution states and terminal fluctuation length.

While crowding-induced changes in molecular conformation are often explained in terms of entropic effects, as described above, crowding molecules can also affect the enthalpic contributions to the free energy change of the molecule from changing conformation. The most relevant enthalpic effect in our case would be due to preferential hydration of the crowder (which would modulate the solvent quality). Two studies have investigated the entropic and enthalpic contributions of different crowders on the stability and aggregation of various proteins and nucleic acids, with varying and often conflicting results (44,45). However, the overwhelming majority of studies using dextran as a crowder have shown that the entropic excluded volume effect dominates the crowding-induced free energy change (44–48).

Further, a very recent study examining crowding-induced protein aggregation (45) has shown that flexible, inert, hydrophilic polysaccharides (such as dextran) influence the conformational free energy solely via excluded volume interactions. Interestingly, this same study shows that the effect of dextran-crowding is not proportional to the solution viscosity, in line with our diffusion results. While one recent experiment (49) reported that the crowding-induced stabilization of the protein ubiquitin by dextran is largely caused by enthalpic rather than entropic effects, this enthalpy-driven stabilization is shown to be independent of the size of the dextran (comparing polymeric to monomeric dextran) and to rely solely on the chemical structure (as expected for an enthalpy-driven process). Conversely, our data show that the size of the dextran plays an important role in the conformational fluctuations of DNA. As crowder size plays a key role in entropically driven processes, our results suggest that entropy rather than enthalpy is indeed the driving force underlying the crowding-induced conformational change of DNA, in line with reported results for conformational changes in proteins.

Surprisingly, despite the initial conformational change induced by the addition of crowders, we see little change in elongation, width distribution, or fluctuation time- and length-scales as the crowder level is increased from $C =$ ~10–40. We see a similar saturating effect for DNA diffusion in S_d, which we attribute to the mobility of S_d as compared to L_d and to the DNA itself. Thus, we can understand the initial mobility reduction and elongation/ordering of the DNA induced by the addition of crowders as driven by entropic depletion effects. However, because dextran is much more mobile than DNA, the DNA is still subject to rapid thermal kicks from the crowders and rapidly changing available space to fluctuate within, which counteracts the slowing and elongation driven by entropy maximization of the crowders. Because L_d is ~6$\times$ slower than S_d, the enhanced elongation in L_d is due to less rapid thermal kicks and rearranging. This reduced mobility also leads to a greater DNA mobility reduction, which is coupled with an exponential

dependence of mobility on crowding level and subdiffusive behavior.

CONCLUSIONS

We have used single-molecule imaging and particle-tracking techniques to simultaneously track molecular diffusion and conformation of large genome-sized DNA in crowded environments that mimic cellular crowding conditions. Despite the essential role that mobility and configuration play in DNA function in the cell, relatively few studies have investigated the effects of crowding on large DNA and no previous studies have experimentally measured both center-of-mass mobility and conformational dynamics to elucidate the connection between the two. We determine the linearity and ergodicity of DNA MSDs and quantify both the probability distributions of DNA elongation states as well as elongation fluctuation time- and length-scales.

While DNA displays ergodic Brownian motion for all crowding cases, we find that underlying diffusive mechanisms of large DNA are driven by the size and mobility of the crowder rather than the DNA itself. For smaller crowders we find classical linear scaling of the MSD with time, which is linked to a novel saturation effect whereby increased levels of crowding beyond ~20% have negligible effect on DNA diffusion, due to the high crowder mobility counteracting the entropic depletion effect restricting DNA conformation and diffusion. Reduced DNA elongation in smaller crowders coupled with a similar unique saturation effect of elongation state distributions and fluctuation timescales further supports this result. In contrast, DNA diffusion in large crowders displays exponential mobility reduction with crowder concentration up to ~300$\times$ at 40%, which is coupled with weak subdiffusive dynamics, with $\alpha \approx 0.7$–0.9, demonstrating that the fractional Brownian motion model for macromolecular diffusion in crowded environments well explains the diffusion of large DNA among crowders that are $\leq 50\times$ smaller and more mobile than the DNA itself.

While DNA size plays a minimal role in diffusion, it dominates elongation dynamics. Both DNA constructs exhibit elongation and slower state fluctuations upon crowding with elongation probabilities that are gamma-distributed and show minimal dependence on crowder concentration. However, 115-kbp DNA displays elongation distribution widths and fluctuation lengths that increase upon crowding, in contrast to 11-kbp DNA in which these parameters actually decrease. Both effects are signatures of the reduced DNA entropy induced by the depletion effect of the surrounding crowders.

Our collective results, which, to our knowledge, reveal important new insights into the complex effects of cellular crowding on large DNA, are critical to a wide range of open questions and problems debated by researchers in biology, physics, chemistry, engineering, materials science, and medicine, including understanding important biological processes, developing new drug delivery and gene therapy techniques, fabricating synthetic cells, and designing novel biomaterials.

SUPPORTING MATERIAL

Two figures are available at http://www.biophysj.org/biophysj/supplemental/S0006-3495(15)00154-X.

AUTHOR CONTRIBUTIONS

C.D.C. was responsible for data analysis, interpretation, and manuscript preparation; S.G. for sample preparation and data collection; and R.M.R.-A. for experiment design, interpretation, and manuscript preparation.

ACKNOWLEDGMENTS

We thank Dr. Douglas E. Smith for useful discussions regarding this project.

This research was funded by the Air Force Office of Scientific Research Young Investigator Program under grant No. FA95550-12-1-0315.

REFERENCES

1. Ellis, R. J. 2001. Macromolecular crowding: an important but neglected aspect of the intracellular environment. *Curr. Opin. Struct. Biol.* 11:114–119.
2. Nakano, S., D. Miyoshi, and N. Sugimoto. 2014. Effects of molecular crowding on the structures, interactions, and functions of nucleic acids. *Chem. Rev.* 114:2733–2758.
3. Miyoshi, D., and N. Sugimoto. 2008. Molecular crowding effects on structure and stability of DNA. *Biochimie.* 90:1040–1051.
4. Tan, C., S. Saurabh, …, P. Leduc. 2013. Molecular crowding shapes gene expression in synthetic cellular nanosystems. *Nat. Nanotechnol.* 8:602–608.
5. Rivas, G., F. Ferrone, and J. Herzfeld. 2004. Life in a crowded world. *EMBO Rep.* 5:23–27.
6. Pelletier, J., K. Halvorsen, …, S. Jun. 2012. Physical manipulation of the *Escherichia coli* chromosome reveals its soft nature. *Proc. Natl. Acad. Sci. USA.* 109:E2649–E2656.
7. Heddi, B., and A. T. Phan. 2011. Structure of human telomeric DNA in crowded solution. *J. Am. Chem. Soc.* 133:9824–9833.
8. Li, G.-W., O. G. Berg, and J. Elf. 2009. Effects of macromolecular crowding and DNA looping on gene regulation kinetics. *Nat. Phys.* 5:294–297.
9. Höfling, F., and T. Franosch. 2013. Anomalous transport in the crowded world of biological cells. *Rep. Prog. Phys.* 76:046602.
10. Sherr, C. J. 1996. Cancer cell cycles. *Science.* 274:1672–1677.
11. Blackburn, E. H. 1991. Structure and function of telomeres. *Nature.* 350:569–573.
12. Herweijer, H., and J. A. Wolff. 2003. Progress and prospects: naked DNA gene transfer and therapy. *Gene Ther.* 10:453–458.
13. Wiethoff, C. M., and C. R. Middaugh. 2003. Barriers to nonviral gene delivery. *J. Pharm. Sci.* 92:203–217.
14. Bally, M. B., P. Harvie, …, D. L. Reimer. 1999. Biological barriers to cellular delivery of lipid-based DNA carriers. *Adv. Drug Deliv. Rev.* 38:291–315.
15. Pastor, I., L. Pitulice, …, F. Mas. 2014. Effect of crowding by dextrans in enzymatic reactions. *Biophys. Chem.* 185:8–13.

16. Dauty, E., and A. S. Verkman. 2005. Actin cytoskeleton as the principal determinant of size-dependent DNA mobility in cytoplasm: a new barrier for non-viral gene delivery. *J. Biol. Chem.* 280:7823–7828.

17. Lukacs, G. L., P. Haggie, …, A. S. Verkman. 2000. Size-dependent DNA mobility in cytoplasm and nucleus. *J. Biol. Chem.* 275:1625–1629.

18. Jones, J. J., J. R. van der Maarel, and P. S. Doyle. 2011. Effect of nanochannel geometry on DNA structure in the presence of macromolecular crowding agent. *Nano Lett.* 11:5047–5053.

19. Zorrilla, S., M. A. Hink, …, M. P. Lillo. 2007. Translational and rotational motions of proteins in a protein crowded environment. *Biophys. Chem.* 125:298–305.

20. Szymanski, J., and M. Weiss. 2009. Elucidating the origin of anomalous diffusion in crowded fluids. *Phys. Rev. Lett.* 103:038102.

21. Regner, B. M., D. Vučinić, …, T. J. Sejnowski. 2013. Anomalous diffusion of single particles in cytoplasm. *Biophys. J.* 104:1652–1660.

22. Weiss, M. 2013. Single-particle tracking data reveal anticorrelated fractional Brownian motion in crowded fluids. *Phys. Rev. E Stat. Nonlin. Soft Matter Phys.* 88:010101.

23. Platani, M., I. Goldberg, …, J. R. Swedlow. 2002. Cajal body dynamics and association with chromatin are ATP-dependent. *Nat. Cell Biol.* 4:502–508.

24. Stiehl, O., K. Weidner-Hertrampf, and M. Weiss. 2013. Kinetics of conformational fluctuations in DNA hairpin-loops in crowded fluids. *New J. Phys.* 15:113010.

25. Kojima, M., K. Kubo, and K. Yoshikawa. 2006. Elongation/compaction of giant DNA caused by depletion interaction with a flexible polymer. *J. Chem. Phys.* 124:024902.

26. Biswas, N., M. Ichikawa, …, K. Yoshikawa. 2012. Phase separation in crowded micro-spheroids: DNA-PEG system. *Chem. Phys. Lett.* 539:157–162.

27. Zhang, C., P. G. Shao, …, J. R. van der Maarel. 2009. Macromolecular crowding induced elongation and compaction of single DNA molecules confined in a nanochannel. *Proc. Natl. Acad. Sci. USA.* 106:16651–16656.

28. Laib, S., R. M. Robertson, and D. E. Smith. 2006. Preparation and characterization of a set of linear DNA molecules for polymer physics and rheology studies. *Macromolecules.* 39:4115–4119.

29. Efron, B., and R. Tibshirani. 1990. Statistical Data Analysis in the Computer Age. Department of Statistics, University of Toronto, Toronto, Ontario, Canada.

30. Chapman, C. D., K. Lee, …, R. M. Robertson-Anderson. 2014. Onset of non-continuum effects in microrheology of entangled polymer solutions. *Macromolecules.* 47:1181–1186.

31. Chapman, C. D., and R. M. Robertson-Anderson. 2014. Nonlinear microrheology reveals entanglement-driven molecular-level viscoelasticity of concentrated DNA. *Phys. Rev. Lett.* 113:098303.

32. Klages, R., G. Radons, and I. M. Sokolov. 2008. Anomalous Transport: Foundations and Applications. John Wiley, New York.

33. He, Y., S. Burov, …, E. Barkai. 2008. Random time-scale invariant diffusion and transport coefficients. *Phys. Rev. Lett.* 101:058101.

34. Cherstvy, A. G., and R. Metzler. 2014. Non-ergodicity, fluctuations, and criticality in heterogeneous diffusion processes. arXiv preprint arXiv:1404.3356.

35. Robertson, R. M., S. Laib, and D. E. Smith. 2006. Diffusion of isolated DNA molecules: dependence on length and topology. *Proc. Natl. Acad. Sci. USA.* 103:7310–7314.

36. Honeycutt, J., D. Thirumalai, and D. Klimov. 1989. Polymer chains in porous media. *J. Phys. Math. Gen.* 22:L169.

37. Baumgärtner, A., and M. Muthukumar. 1987. A trapped polymer chain in random porous media. *J. Chem. Phys.* 87:3082–3088.

38. Robertson, R. M., and D. E. Smith. 2007. Strong effects of molecular topology on diffusion of entangled DNA molecules. *Proc. Natl. Acad. Sci. USA.* 104:4824–4827.

39. Chapman, C. D., S. Shanbhag, …, R. M. Robertson-Anderson. 2012. Complex effects of molecular topology on diffusion in entangled biopolymer blends. *Soft Matter.* 8:9177–9182.

40. Doi, M., and S. F. Edwards. 1986. The Theory of Polymer Dynamics. Oxford University Press, New York.

41. Arkın, H., and W. Janke. 2013. Gyration tensor based analysis of the shapes of polymer chains in an attractive spherical cage. *J. Chem. Phys.* 138:054904.

42. Phelps, C., W. Lee, …, A. H. Marcus. 2013. Single-molecule FRET and linear dichroism studies of DNA breathing and helicase binding at replication fork junctions. *Proc. Natl. Acad. Sci. USA.* 110:17320–17325.

43. Raghu, R. C., and J. Schofield. 2012. Simulation of tethered oligomers in nanochannels using multi-particle collision dynamics. *J. Chem. Phys.* 137:014901.

44. Hall, D., and A. P. Minton. 2003. Macromolecular crowding: qualitative and semiquantitative successes, quantitative challenges. *Biochim. Biophys. Acta.* 1649:127–139.

45. Breydo, L., K. D. Reddy, …, V. N. Uversky. 2014. The crowd you're in with: effects of different types of crowding agents on protein aggregation. *Biochim. Biophys. Acta.* 1844:346–357.

46. Goodrich, G. P., M. R. Helfrich, …, C. D. Keating. 2004. Effect of macromolecular crowding on DNA:Au nanoparticle bioconjugate assembly. *Langmuir.* 20:10246–10251.

47. Christiansen, A., and P. Wittung-Stafshede. 2014. Synthetic crowding agent dextran causes excluded volume interactions exclusively to tracer protein apoazurin. *FEBS Lett.* 588:811–814.

48. Wang, Y., M. Sarkar, …, G. J. Pielak. 2012. Macromolecular crowding and protein stability. *J. Am. Chem. Soc.* 134:16614–16618.

49. Senske, M., L. Törk, …, S. Ebbinghaus. 2014. Protein stabilization by macromolecular crowding through enthalpy rather than entropy. *J. Am. Chem. Soc.* 136:9036–9041.